An investigation of uncertainty in impact testing

Hyo Soo Kim and Tony L. Schmitz
Department of Mechanical and Aerospace Engineering
University of Florida
Gainesville, FL

Abstract
This paper evaluates uncertainty contributors for frequency response function (FRF) measurements obtained through impact testing. The FRF is an important estimator for the structural dynamics of tool-holder-spindle-machine assemblies and is used as input to analyses of milling dynamics. Therefore, it is of interest to determine the confidence in the measurement results. In this work, we present a bivariate uncertainty analysis that considers statistical variations, imperfect calibration coefficients for the hammer and transducer, misalignment between the intended and actual force direction during impact, and mass loading (when using an accelerometer). An ellipsoid-shaped confidence region (at each frequency) is defined in the complex plane.

Keywords:
Frequency response function, bivariate, ellipsoid, cosine error, mass loading

1 INTRODUCTION

In this paper we identify and combine primary uncertainty contributors for tool point frequency response function (FRF) measurements completed using impact testing. By impacting the free end of the tool-holder-spindle-machine assembly with an instrumented hammer, a wide range of frequencies can be excited simultaneously. The resulting response is typically recorded using a low mass accelerometer, although non-contact transducers are also sometimes applied. The time domain responses are (Fourier) transformed into the frequency domain and the complex ratio of the vibration response to the input force is calculated to determine the assembly FRF. We focus on impact testing because it is the most common method used to quickly identify the tool point FRF required for milling process dynamics analyses.

The paper is organized as follows. First, a statistical analysis of multiple impacts is completed where the bivariate nature of the complex data is respected. Next, the transducer calibration coefficient uncertainty is considered. Then, the errors caused by incorrect force direction and accelerometer mass loading are explored. Finally, the overall uncertainty is identified. The reader may note that this paper does not address sampling, filtering, or windowing issues and assumes that the voltages output by the transducers represent accurate estimates of the tool point dynamics, except for the uncertainty sources identified here.

STATISTICAL ANALYSIS

In this section we explore the statistical variation of multiple, single impact FRFs obtained from tests performed on a 19 mm diameter carbide rod inserted in a shrink fit tool holder (clamped in an HSK-63A spindle). Because the FRF is a complex-valued (or bivariate) function, an ellipsoidal uncertainty region with a 95% confidence level is identified at each frequency, rather than the more traditional single-dimensional confidence interval. The ellipsoidal region is defined by [1]:

$$\left(\bar{x}-\mu\right)^T V^{-1}\left(\bar{x}-\mu\right) \le \frac{(n-1)p}{n-p} F_{\alpha;p,(n-p)}, \quad (1)$$

where, $\bar{x}$ is the vector of frequency-dependent mean values of the real and imaginary components of the sample FRFs, μ is the outer points of the confidence region that define the ellipsoidal boundary, V is the covariance matrix, n is the number of samples, $F_{\alpha;p,(n-p)}$ is the statistic of the F distribution with p and n-p degrees of freedom, the probability $1-\alpha(\alpha-1)$, (α = 0.05 for 95% confidence) is the level of significance, and p is the number of variates (p = 2 for our analysis). Also, Eq. 1 assumes normal distributions.

As shown in Eq. 1, the covariance matrix, which includes the standard variances of the real and imaginary FRF components as well as the estimated covariance between them, plays an important role in obtaining the ellipsoid uncertainty region. The following steps follow the analysis detailed in [2] for constructing the covariance matrix.

The standard uncertainties of the real and imaginary components are determined from Eqs. 2 and 3, where $\overline{\mathrm{Re}(FRF)}$ and $\overline{\mathrm{Im}(FRF)}$ are the means of n test samples at each frequency. The estimated covariance between $\mathrm{Re}(FRF)$ and $\mathrm{Im}(FRF)$ is calculated using Eq. 4.

$$u(\mathrm{Re}(FRF)) = \sqrt{\frac{1}{n(n-1)}\sum_{i=1}^{n}\left[\mathrm{Re}(FRF_i)-\overline{\mathrm{Re}(FRF)}\right]} \quad (2)$$

$$u(\mathrm{Im}(FRF)) = \sqrt{\frac{1}{n(n-1)}\sum_{i=1}^{n}\left[\mathrm{Im}(FRF_i)-\overline{\mathrm{Im}(FRF)}\right]} \quad (3)$$

$$u\left(\mathrm{Re}\left(FRF\right),\mathrm{Im}\left(FRF\right)\right) = \frac{1}{n(n-1)}\sum_{i=1}^{n}\left[\mathrm{Re}(FRF_i)-\overline{\mathrm{Re}(FRF)}\right]\left[\mathrm{Im}(FRF_i)-\overline{\mathrm{Im}(FRF)}\right] \quad (4)$$

The covariance matrix is constructed by setting the on-diagonal terms of the (2 x 2) matrix equal to the standard variances of the real and imaginary components and the off-diagonal terms equal to the covariance.

$$V = \begin{pmatrix} u^2[\mathrm{Re}(FRF)] & u[\mathrm{Re}(FRF),\mathrm{Im}(FRF)] \\ u[\mathrm{Im}(FRF),\mathrm{Re}(FRF)] & u^2(\mathrm{Im}(FRF)) \end{pmatrix} \quad (5)$$

Note that each of the results in Eqs. 1-5 are frequency-dependent; a new value is defined for each frequency within the measurement range of interest. Figure 1 shows the mean FRF and the ellipsoidal uncertainty regions for 100 single impact tests carried out on the representative tool; the data is displayed in the complex plane. The reader may note that this is the voltage data only. The calibration coefficients are applied and their uncertainties treated in the next section. The small elliptical uncertainty regions indicate the measurements are highly repeatable.

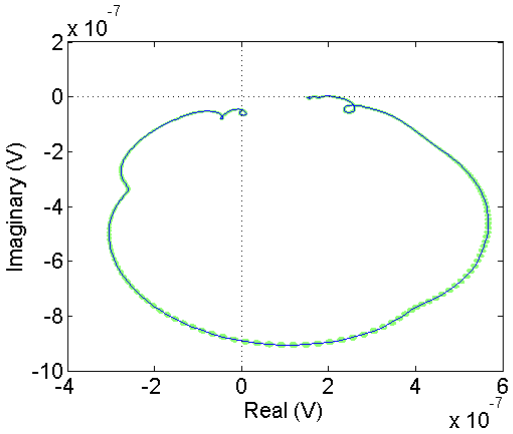

Figure 1: Nyquist plot of the mean FRF with ellipsoidal uncertainty regions (95% confidence level).

CALIBRATION COEFFICIENT UNCERTAINTY

In order to convert the measured voltages to appropriate engineering units, the calibration coefficients must be applied. In this section, we combine the inherent uncertainty in these values with the statistical measurement variation shown in the previous section. The FRF is expressed in terms of the calibration coefficients, C_x and C_f, for the accelerometer (or other transducer) and hammer and the corresponding voltages, V_x and V_f, by:

$$FRF = \frac{C_x V_x}{C_f V_f}. \tag{6}$$

For the accelerometer and hammer applied in this study, the manufacturers provided ranges of ±1% for C_x and ±2.7% for C_f. The standard uncertainties were estimated from these ranges by selecting an appropriate distribution. We assumed a uniform distribution with 100% confidence that the actual value falls within the specified range for both coefficients [3].

$$u(C_x) = \frac{0.01 C_x}{\sqrt{3}} \tag{7}$$

$$u(C_f) = \frac{0.027 C_f}{\sqrt{3}} \tag{8}$$

Uncertainty in the calibration coefficients was included using a bivariate form of the Gaussian error propagation law [4]; a brief review of this method is now provided. Consider an arbitrary measurement function:

$$y = f(X) = f(x_1, x_2, ..., x_m) \tag{9}$$

that describes the relationship between a complex-valued quantity of interest, the measurand y, and m influence quantities. The function f is comprised of two scalar functions, f_1 and f_2, that evaluate the real and imaginary parts, respectively (i.e., $y = f_1(X) + f_2(X)$). The uncertainty in the values assigned to the input quantities x_1 to x_m is given by the ($2m$ x $2m$) matrix:

$$V(X) = \begin{pmatrix} u^2(x_{11}) & u(x_{11},x_{21}) & \cdots & u(x_{11},x_{1m}) & u(x_{11},x_{2m}) \\ x(x_{21},x_{11}) & u^2(x_{21}) & \cdots & u(x_{21},x_{1m}) & u(x_{21},x_{2m}) \\ \vdots & \vdots & \ddots & \vdots & \vdots \\ u(x_{1m},x_{11}) & u(x_{1m},x_{21}) & \cdots & u^2(x_{1m}) & u(x_{1m},x_{2m}) \\ u(x_{2m},x_{11}) & u(x_{2m},x_{21}) & \cdots & u(x_{2m},x_{1m}) & u^2(x_{2m}) \end{pmatrix} \tag{10}$$

where the on-diagonal terms represent the standard variance of the associated inputs and the off-diagonal terms represent the covariance. Also, the first subscript for each term indicates the real (1) or imaginary (2) part of the selected input quantity. The uncertainty in y is expressed using a (2 x 2) covariance matrix:

$$V(y) = J(y) V(X) J(y)^T, \tag{11}$$

where $J(y)$ is the (2 x 2m) Jacobian matrix of the scalar parts of f with respect to the scalar elements of X:

$$J(y) = \begin{pmatrix} \frac{\partial f_1}{\partial x_{11}} & \frac{\partial f_1}{\partial x_{21}} & \frac{\partial f_1}{\partial x_{12}} & \frac{\partial f_1}{\partial x_{22}} & \cdots & \frac{\partial f_1}{\partial x_{1m}} & \frac{\partial f_1}{\partial x_{2m}} \\ \frac{\partial f_2}{\partial x_{11}} & \frac{\partial f_2}{\partial x_{21}} & \frac{\partial f_2}{\partial x_{12}} & \frac{\partial f_2}{\partial x_{22}} & \cdots & \frac{\partial f_2}{\partial x_{1m}} & \frac{\partial f_2}{\partial x_{2m}} \end{pmatrix}. \tag{12}$$

In [4], a convenient approach to obtaining $J(y)$ is introduced. The Jacobian matrix is described using a (2 x 2) block structure that can be associated with the derivatives of f with respect to individual bivariate inputs:

$$J(y) = \begin{bmatrix} J_1(y) & J_2(y) & \cdots & J_m(y) \end{bmatrix}, \text{ where} \tag{13}$$

$$J_i(y) = \begin{bmatrix} \frac{\partial f_1}{\partial x_{1j}} & \frac{\partial f_1}{\partial x_{2j}} \\ \frac{\partial f_2}{\partial x_{1j}} & \frac{\partial f_2}{\partial x_{2j}} \end{bmatrix}. \tag{14}$$

These blocks represent the bivariate sensitivity coefficients for the analysis. They can be related directly to the complex partial derivatives of f by a matrix representation for complex numbers. For any complex number $z \equiv a + jb$, the mapping:

$$M(z) \equiv \begin{bmatrix} a & -b \\ b & a \end{bmatrix} \tag{15}$$

generates a (2 x 2) matrix representation for z. Such matrices behave as complex numbers under the usual matrix operations and, provided the complex function $f(z)$ is analytic in the region of interest, the Cauchy-Riemann relations apply to its partial derivatives so that:

$$\frac{\partial f_1}{\partial a} = \frac{\partial f_2}{\partial b} \text{ and } \frac{\partial f_1}{\partial b} = \frac{\partial f_2}{\partial a}. \tag{16}$$

Using Eqs. 15 and 16, the full Jacobian matrix is:

$$J(y) = \begin{bmatrix} M\left(\frac{\partial f}{\partial x_1}\right) & M\left(\frac{\partial f}{\partial x_2}\right) & \cdots & M\left(\frac{\partial f}{\partial x_m}\right) \end{bmatrix}. \tag{17}$$

For the calibration coefficients, three uncertain input variables were considered in Eq. 6. Here, we have set the frequency domain voltage ratio V_x/V_f equal to V_r:

$$y = FRF = f(V_r, C_x, C_f)\,. \tag{18}$$

The first step was to construct the input covariance matrix, where the upper left (2 x 2) terms depend on the statistical evaluation of the measured V_r and no correlation was considered between the real-valued accelerometer and hammer calibration coefficients.

$$V(x) = \begin{pmatrix} u^2[\mathrm{Re}(V_r)] & u[\mathrm{Re}(V_r),\mathrm{Im}(V_r)] & 0 & 0 & 0 & 0 \\ u[\mathrm{Im}(V_r),\mathrm{Re}(V_r)] & u^2[\mathrm{Im}(V_r)] & 0 & 0 & 0 & 0 \\ 0 & 0 & u^2[\mathrm{Re}(C_x)] & 0 & 0 & 0 \\ 0 & 0 & 0 & 0 & 0 & 0 \\ 0 & 0 & 0 & 0 & u^2(\mathrm{Re}(C_f)) & 0 \\ 0 & 0 & 0 & 0 & 0 & 0 \end{pmatrix} \tag{19}$$

Next, the Jacobian matrix was determined using Eq. 20. The output covariance matrix was then computed using Eq. 11. Finally, the ellipsoidal uncertainty region was defined using Eq. 1; see Fig. 2. It is observed that the relative influence of calibration coefficients is much larger than the statistical measurement variation and is, in fact, the largest contributor for the case presented here.

$$J(y) = \left(M\left(\frac{\partial FRF}{\partial V_r}\right), M\left(\frac{\partial FRF}{\partial C_x}\right), M\left(\frac{\partial FRF}{\partial C_f}\right) \right). \tag{20}$$

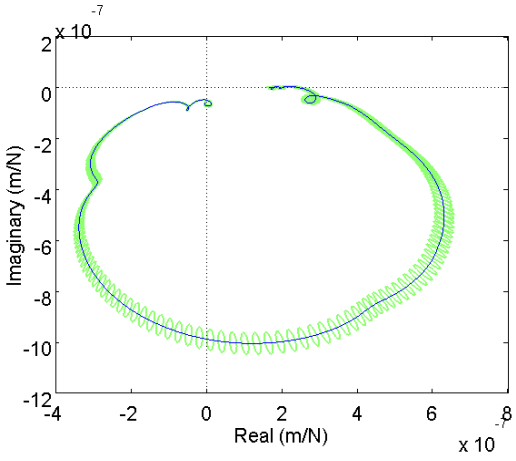

Figure 2: Ellipsoidal uncertainty region including the statistical variation and calibration coefficients.

COSINE ERROR

During impact tests, the force input direction is generally not perfectly aligned with the sensor direction. This leads to the well-known cosine error and subsequent bias. Any misalignment between the force and sensor directions causes the force which actually excites the system to be less than the force sensed by the hammer load cell.

To evaluate typical force direction misalignment angles, tests were performed on a force dynamometer by three users in the three Cartesian directions. The misalignment angle, β, between the actual and intended direction for these tests was calculated from the dot product of the norms of the force along the selected axis and the resultant force; Eq. 21 depicts the x direction case. The mean angle for the three testers was 3.0 deg.

$$\beta = \cos^{-1}\left(\frac{F_x \cdot F_h}{|F_x||F_h|}\right) \tag{21}$$

Due to the angular misalignment, the FRF amplitude is under estimated (biased). The true FRF, FRF_t, should be determined from the force component in the transducer direction, F_t. However, the measure FRF is actually computed using the force reported by the hammer load cell, F_h. The bias correction is realized using Eq. 23 [5], where u(β) is the standard uncertainty in the misalignment angle. Here we have assumed a standard uncertainty equal to the mean value of 3.0 deg. Figure 3 shows the measure and corrected FRF magnitudes. It is seen that the bias is quite small for this typical case.

$$FRF_t = \frac{X}{F_t}, \qquad FRF_h = \frac{X}{F_h} \tag{22}$$

$$FRF_t = \frac{X}{F_t} = \frac{X}{F_h\left(1-\frac{1}{2}u^2(\beta)\right)} = FRF_h\left(1-\frac{1}{2}u^2(\beta)\right)^{-1} \tag{23}$$

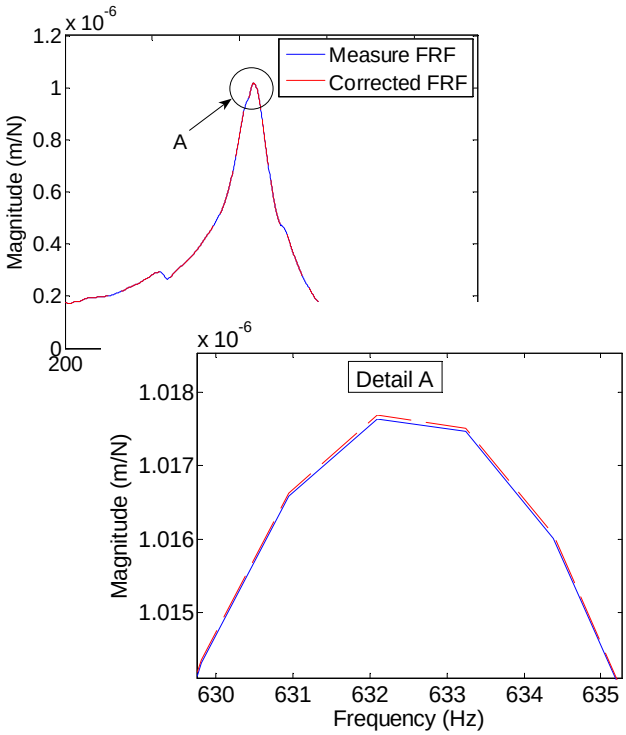

Figure 3: Measure and corrected FRFs. It is seen that cosine error leads to an underestimated magnitude.

Since the misalignment angle is not perfectly known, uncertainty propagation can be performed using the Gaussian uncertainty propagation law. The measurand was obtained by replacing F_t in the denominator of the FRF_t equation with $F_h\cos(\beta)$. The bivariate error propagation was then carried out on two input variables: the measured FRF including calibration coefficient uncertainty and the misalignment angle.

$$FRF_t = f(FRF_h, \beta) \tag{24}$$

The same steps described in the previous section were again followed. First, the input covariance matrix was written as:

$$V(x) = \begin{pmatrix} u^2[\mathrm{Re}(FRF_h)] & u[\mathrm{Re}(FRF_h),\mathrm{Im}(FRF_h)] & 0 & 0 \\ u[\mathrm{Im}(FRF_h),\mathrm{Re}(FRF_h)] & u^2[\mathrm{Im}(FRF_h)] & 0 & 0 \\ 0 & 0 & u^2[\mathrm{Re}(\beta)] & 0 \\ 0 & 0 & 0 & 0 \end{pmatrix} \tag{25}$$

Next, the Jacobian matrix was described by Eq. 26. Finally, the output covariance matrix was computed using Eq. 11 and the ellipsoidal uncertainty region was defined using Eq. 1; see Fig. 4. By comparison to Fig. 2, it is seen that the uncertainty contribution is quite small.

$$J(y) = \left(M(\frac{\partial FRF_t}{\partial FRF_h}), M(\frac{\partial FRF_t}{\partial \beta}) \right). \quad (26)$$

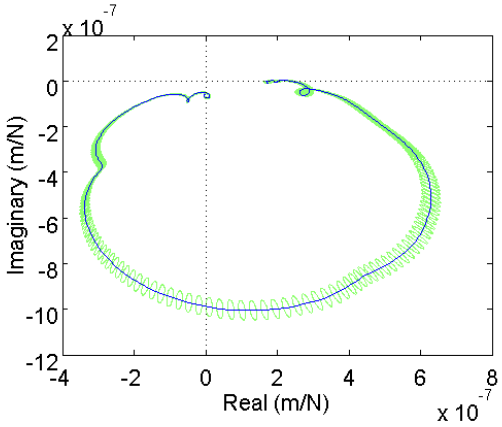

Figure 4: Ellipsoidal uncertainty regions including cosine error, statistical variation, and calibration coefficients.

MASS LOADING EFFECT

Because the tool point dynamics are modified when the accelerometer is attached, the accelerometer mass must be considered. To correct the mass loading bias, we applied Eq. 27 [6], where m_a is the accelerometer mass (0.93 mg with range of $\pm 1\%$), A_i indicates accelerance, or the complex ratio of acceleration to input force, and the *c* and *m* subscripts denote corrected and measured, respectively. Even though the bias is removed using this approach, uncertainty remains in the corrected result. Again, the ellipsoidal uncertainty region was established using the Gaussian uncertainty propagation law. To carry out the analysis, we converted the accelerance terms in Eq. 27 to receptances (complex displacement to force) using $A_i = -\omega^2 R_i$, where ω is the frequency (in rad/s) and R_i is the receptance. See Eq. 28.

$$A_c = \frac{A_m}{1 - m_a A_m} \quad (27) \qquad R_c = \frac{R_m}{1 + m_a \omega^2 R_m} \quad (28)$$

Note that the measured response in Eq. 28 is actually the corrected response from the cosine error analysis, which includes the uncertainties due to the statistical variation and calibration coefficients. The input variables to the propagation law were R_m (or FRF_t, the corrected response from cosine error) and m_a. The input covariance matrix was given by Eq. 30. The Jacobian matrix was computed and the same steps were again followed to identify the final frequency-by-frequency ellipsoidal uncertainty regions. See Fig. 5; the relative uncertainty contribution is again small.

$$R_c = f(FRF_t, m_a) \quad (29)$$

$$V_x = \begin{pmatrix} u^2[\mathrm{Re}(FRF_t)] & u[\mathrm{Re}(FRF_t), \mathrm{Im}(FRF_t)] & 0 & 0 \\ u[\mathrm{Im}(FRF_t), \mathrm{Re}(FRF_t)] & u^2[\mathrm{Im}(FRF_t)] & 0 & 0 \\ 0 & 0 & u^2[\mathrm{Re}(m_a)] & 0 \\ 0 & 0 & 0 & 0 \end{pmatrix} \quad (30)$$

$$J(y) = \left[M\left(\frac{\partial FRF_c}{\partial FRF_t}\right), M\left(\frac{\partial FRF_c}{\partial m_a}\right) \right] \quad (31)$$

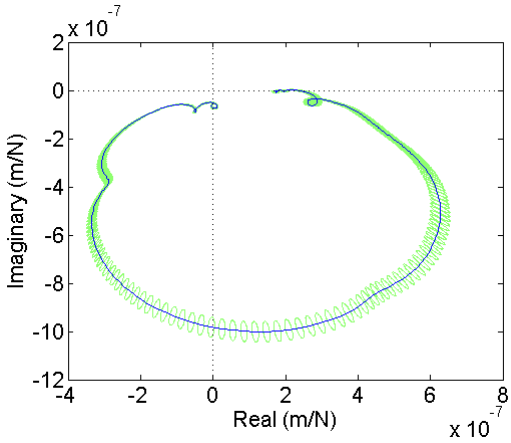

Figure 5: Final uncertainty including statistical variation, calibration coefficients, cosine error, and mass loading.

CONCLUSIONS

In this work we evaluated uncertainty contributors for FRF measurements obtained using impact testing. We presented a bivariate uncertainty analysis that considered statistical variations, calibration coefficients, misalignment between the intended and actual force direction, and mass loading. An ellipsoidal confidence region at each frequency was defined in the complex plane. Additionally, the biases introduced by the hammer/vibration transducer misalignment and accelerometer mass loading were corrected.

ACKNOWLEDGMENTS

This work was supported by the National Science Foundation (DMI-0555645 and DMI-0238019) and the Korea Science and Engineering Foundation (D00010). The authors also wish to acknowledge Dr. T. Schultz.

REFERENCES

1. Jobson J.D., (1992), *Applied Multivariate Data Analysis*, Springer-Verlag, NJ.
2. Ridler, N.M., Salter, M.J., (2002), "An Approach to the Treatment of Uncertainty in Complex S-parameter Measurements," *Metrologia*, Vol. 39, pp. 295-302.
3. Taylor, B.N. and C.E. Kuyatt, (1994), "Guidelines for Evaluating and Expressing the Uncertainty of NIST Measurement Results", *NIST Technical Note 1297 1994 Edition*.
4. Hall B.D., (2004), "On the Propagation of Uncertainty in Complex-valued Quantities", *Metrologia*, Vol. 41, pp. 173-177.
5. International Standards Organization (ISO), (1993), *Guide to the Expression of Uncertainty in Measurement* (Corrected and Reprinted 1995).
6. Ashory, M., (1999), *High Quality Modal Testing Methods*, Ph.D. Dissertation, Imperial College of Science, Technology, and Medicine, London.